Gain Enhancement of an UWB Antenna Based on a FSS Reflector for Broadband Applications

Avula Swetha* **and Kurukundu R. Naidu**

Abstract—In this paper, a novel semi-circular ultra wide-band antenna inspired by a complementary split ring resonator for enhancement of bandwidth and a frequency selective surface reflector for gain enhancement is proposed for broadband applications. Initially, an ultra wide-band antenna employing a pair of L-shaped resonators and complementary split ring resonators is proposed which provides a wide impedance bandwidth of 130.3% from 3.16 to 15 GHz with -10 dB return loss. Finally, a frequency selective surface reflector is employed below the suggested ultra wide-band antenna to enhance the gain. The dimensions of the coplanar waveguide fed ultra wide-band antenna are $35 \times 30 \times 1.6$ mm^3, and those of the ultra wide-band antenna with a frequency selective surface reflector, which consists of 10×10 array of elements located at a distance of 17 mm below the proposed antenna, are $53.15 \times 53.15 \times 1.6$ mm^3. A parametric analysis of substrate dimensions of ultra wide-band antenna and the distance between ultra wide-band antenna and frequency selective surface reflector is performed. The average peak gain of the proposed antenna increases from 4.9 dB to 10.9 dB, which operates at 3.79 GHz, 4.44 GHz, 7.89 GHz, 9.01 GHZ, and 11.15 GHz proposed for broadband applications. With the help of ANSYS, the signal correlation of the proposed antenna is analysed by time domain analysis using similar antennas in face-to-face and side-to-side scenarios. The simulated results of the proposed model are in correlation with experimental ones of the prototype model.

1. INTRODUCTION

The design of an antenna is a challenging task in the implementation of entire wireless mobile systems. Moreover, the fast development of mobile systems towards the fifth generation (5G systems) requires wide band and high gain ultra wide-band (UWB) antennas to fulfil mobile and wireless needs so that complete device dimensions are obtained, and cost and system complexity are reduced. To fulfil the challenging situations of wireless communication, several efforts have been made to discover new antenna geometries [1–3]. Researchers have expressed a keen interest in UWB systems owing to advantages such as a low power consumption, low complexity, and high bandwidth for wireless communication applications [4]. The Federal Communications Commission allotted a spectrum from 3.1 GHz to 10.6 GHz for UWB systems issued in February 2002 [5]. To acquire a UWB antenna with an enhanced bandwidth, several methods have been implemented in literature. In [6–8], various slot resonators were etched on the printed slot antenna to achieve impedance bandwidths of 82.5%, 122%, and 92.7%. In [9–11], a compact UWB antenna designed to achieve impedance bandwidths of 129%, 118.8%, and 129.1% was achieved. In UWB systems, monopole antennas as a radiator exhibit an omnidirectional radiation pattern. Due to its very high back lobe radiation, the peak gain of a UWB antenna is low. To improve the directionality and gain of a UWB antenna and to minimize back lobe radiations, a frequency selective surface(FSS) reflector was employed below the antenna [12, 13]. Ram Krishna and Kumar [12] suggested two different FSS layers to enhance the gain up to 2–4 dB. Kundu et

* Corresponding author: Avula Swetha (swetha0610@gmail.com).
The authors are with the Department of ECE, JNTUA, Ananthapuramu-515002, Andhra Pradesh, India.

al. [14] proposed an antenna loaded with a metamaterial FSS reflector to enhance the gain by 3–4 dB. Ranga et al. [15], proposed a UWB antenna with a reflector placed at 10 mm to enhance the gain up to 1.5 dB throughout the UWB frequency. In [16], a UWB antenna with a one-layer reconfigurable FSS reflector was proposed for multi-band operations. In [17–21], a UWB antenna with an FSS reflector was proposed to achieve the high gain proposed in broadband applications. The proposed UWB antenna is compared with certain broadband-based antennas in the literature, in Table 1.

Table 1. Characteristics of the proposed UWB antenna with certain broadband-based studies.

Ref No	Size ($l \times w \times h$) in mm	ε_r	Bands operated	Peak Gain (dB)	Bandwidth enhancement (%)	Verification of permittivity property	Impedance bandwidth enhancement (GHz)	Operating frequency range (GHz)
[6]	24.5×24.5×1	4.6	4	3.96	122	No	9.15	2.95 to 12.1
[7]	37×37×1.6	4.4	2	4	82.5	No	3.12	2.23 to 5.35
[8]	24×20×1	4.6	2	4.7	92.7	No	6.4	3.7 to 10.1
[9]	28×28×0.8	4.4	4	4.2	129.6	No	9.85	2.7 to 12.5
[10]	50× 22.5×1.5	2.3	2	3	118.8	No	8.2	2.8 to 11
[11]	12×16×1.6	4.4	4	2.6	129.1	No	10.2	2.8 to 13
Proposed work	35×30×1.6	4.4	5	4.9	130.3	Yes	11.84	3.16 to 15

The characteristics of the proposed UWB antenna based on an FSS reflector are compared with those of previously proposed FSS reflectors, listed in Table 2.

Table 2. Characteristics of the proposed UWB antenna with certain FSS reflectors based studies.

Ref No	Size of UWB antenna in mm ($l \times w \times h$)	Size of FSS reflector ($l \times w \times h$) in mm	Bands operated	Peak Gain (dB)	Time response analysis	Bandwidth (GHz)
[13]	72×72×0.508	115×115×0.635	3	9.5	No	3–11
[14]	35×30×0.8	44×44×32.7	4	8.5	No	3.05–13.4
[15]	30×60×0.787	75×105×1.6	4	8	No	3–11.6
[17]	10×12×0.8	102×102×1.6	5	7.5	No	3.5–13
[19]	25×25×1.6	124×124×1.6	2	8.2	No	6.5–9.5
[20]	15.8×14.7×1.6	45×45×1.6	3	8.82	No	4.93–11.72
Proposed work	35×30×1.6	53.15×53.15×1.6	5	10.9	Yes	3.16–15

To meet the requirements of wireless communication, especially for broadband applications, an antenna with a wide bandwidth, high radiation efficiency, and very high peak gain is required. In this study, to meet the above requirements, a novel semi-circular broadband UWB antenna inspired by a pair of L-shaped resonators and complementary split ring resonators (CSRRs) was designed which provided a wide impedance bandwidth of 130.3% from 3.16 to 15 GHz with −10 dB return loss. Later, the radiation efficiency and average peak gain of the proposed CPW-fed UWB antenna based on an FSS reflector increased from 20% to 90.1% and 4.9 dB to 10.9 dB, respectively. Furthermore, a compact CPW-fed UWB antenna based on an FSS reflector's time domain characteristics was designed by using ANSYS HFSS 17. To enhance the impedance bandwidth, a pair of L-shaped resonators and a pair of CSRRs were proposed. To enhance gain, an FSS reflector was placed below the UWB antenna. The prototype model of the antenna was fabricated, tested, and compared with experimental results.

2. ANTENNA CONSTRUCTION

Three iterations of the antenna were explored. In iteration 1, a CPW-fed semi-circular UWB antenna (Antenna-1) was designed with a radius (R_1) of 7.5 mm (Fig. 1). To offer perfect impedance matching, a feed line width (W_F) of 3.5 mm was chosen. The suggested antenna having the dimensions of $35 \times 30 \times 1.6$ mm^3 was fed with a 50 Ω CPW feeding technique printed on an FR4E poxy substrate with a dielectric constant of 4.4. In the second iteration (Antenna-2), to provide symmetry in construction of the UWB antenna, a pair of L-shaped resonators was employed on the back end of the substrate, and a pair of CSRRs was etched on the ground plane to achieve a wide impedance bandwidth of 130.3% from 3.16 to 15 GHz with −10 dB return loss. Finally, in the third iteration (Antenna-3), an FSS reflector having $53.15 \times 53.15 \times 1.6$ mm^3 was constructed on an FR4 substrate with a 10×10 array of elements and employed at a height (h_1) of 17 mm to achieve the peak gain increased from 4.9 dB to 10.9 dB. The analysis of the unit cell of the CSRR, steps for obtaining a broadband, and the FSS reflector principles used to enhance the gain of the antenna are discussed in Sections 2.1, 2.2, and 2.3, respectively.
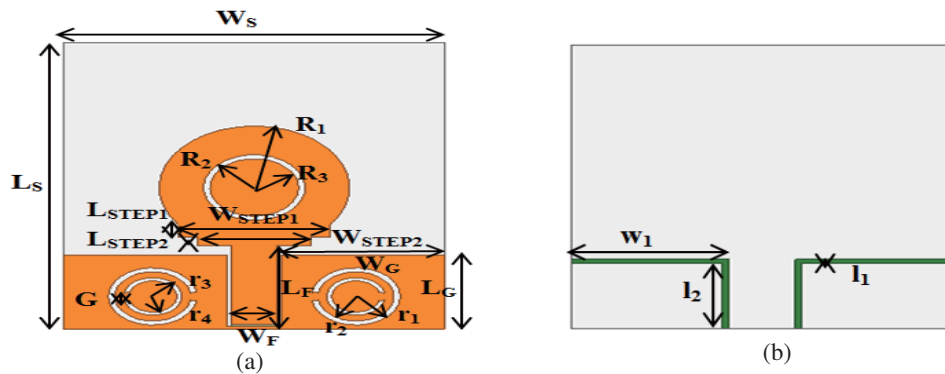

Figure 1. Geometrical dimensions of iteration 2 (Antenna-2) of the semi-circular UWB antenna (a) top, and (b) bottom views.

2.1. Construction of the CSRR Unit Cell

Metamaterials are artificial materials that do not exist in nature; however, they are constructed with unique structures that allow them to exhibit either negative permittivity or permeability or both, which impacts antenna performance characteristics. To enhance antenna characteristics, the effect of either a double negative or single negative material is required. A CSRR is the complement of a split ring resonator (SRR) and is excited by electric field intensity, whereas the SRR is excited by magnetic field intensity. The outer slot of a CSRR is constructed with radii "r_1" and "r_2" whereas the inner slot of the CSRR is designed with radii "r_3" and "r_4", and the gap between CSRRs is considered as "G". The construction of a unit cell of the CSRR and its equivalent circuit [22] are shown in Figs. 2(a) and 2(b). The extraction of the permittivity (ε) of a CSRR based on the Nicholson-Ross-Weir (NRW) technique [23] is shown in Fig. 3(a), which illustrates the waveguide setup analysis used to extract S parameters from which negative permittivity [24] is obtained as represented in Fig. 3(b). To extract S parameters suitable boundary conditions and excitations are assigned on the surface of a three-dimensional unit cell of a CSRR. The metamaterial (CSRR) of a unit cell waveguide analysis setup is achieved by assigning a magnetic conductor on the top and bottom sides of the box, a perfect electric conductor on the split side, and a wave port to another end of the unit cell. The capacitance of the CSRR (C_{CSRR}) is governed by the slot between the metal strips, and a metal strip between the slots governs inductance of CSRR (L_{CSRR}). The dimensions of a unit cell of CSRR $L_X \times L_Y$ is 8×8 mm^2 represented in Fig. 2(a) whereas the dimensions of a unit cell waveguide analysis setup of CSRR $dx \times dy \times dz$ is $44 \times 44 \times 41.6$ mm^3 represented in Fig. 3(a). Thus, the CSRR resonance frequency (f_{CSRR}) is calculated using Eqs. (1)–(5) [25].

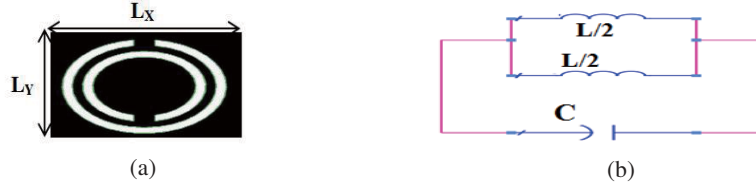$$f_{CSRR} = \frac{1}{2\pi\sqrt{L_{CSRR}C_{CSRR}}} \tag{1}$$

(a)   (b)

Figure 2. (a) Unit cell structure and, (b) equivalent circuit.
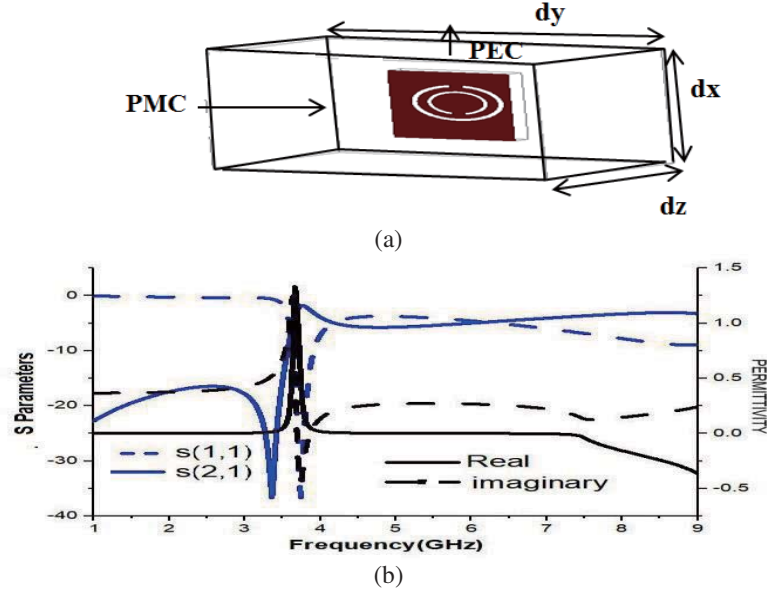

(a)

(b)

Figure 3. (a) Waveguide analysis of a unit cell and, (b) S parameter and permittivity of the CSRR.

$$C_{CSRR} = \frac{N-1}{2}\left[2L - (2N-1)(W+S)\right]C_0 \tag{2}$$

$$C_0 = \varepsilon_0 \frac{K\left(\sqrt{1-k^2}\right)}{K(k)} \quad \text{and} \quad k = \frac{S/2}{W+S/2} \tag{3}$$

$$L_{CSRR} = 4\mu_0\left[L - (N-1)(W+S)\right]\left[\ln\left(\frac{0.98}{\rho}\right) + 1.84\rho\right] \tag{4}$$

$$\rho = \frac{(N-1)(W+S)}{1-(N-1)(W+S)} \tag{5}$$

Here, N is the number of CSRR rings, L the average length of the CSRR ring, W the width of the slot and equal to 0.5 mm, S the distance between the slots and equal to 0.5 mm, and $K(k)$ the first order elliptic integral of k. The above equation is only useful for $N = 2, 3\ldots$ For $N = 2$ (Second ring CSRR) $L = \frac{2r_2+W}{2} = 3.25$ mm. Hence, $L_{CSRR} = 7.79 \times 10^{-8}\,(Henry)$ and $C_{CSRR} = 2.42 \times 10^{-14}\,(Farad)$. Therefore, the resonance frequency of CSRR is $f_{CSRR} = \frac{1}{2\pi\sqrt{L_{CSRR}C_{CSRR}}} = 3.7$ GHz. From this analysis, the calculated value is 3.7 GHz, which is approximately equal to simulated value of 3.79 GHz that specifies that a negative permittivity is obtained and represented in Fig. 3(b).

2.2. Broadband Generation

A thicker substrate is required to enhance the radiating power, diminish the conductor loss, and increase impedance-bandwidth (BW) of the antenna, which is proportional to the thickness of a substrate (h). Therefore, to enhance the bandwidth of a radiating patch, the thickness of substrate is increased.

However, it is impossible to increase 'h', which has a limit represented in Eq. (6) to reduce surface waves.

$$\frac{h}{\lambda_0} \leq \frac{0.3}{2\pi\sqrt{\varepsilon_r}} \tag{6}$$

These surface waves come into the picture because of fringing fields from the edges, which focus the radiation towards the surface. This is not the desired direction, as the antenna must radiate towards the broadside. If the antenna radiates along the surface, radiation is wasted. A conflict arises between enhancing the bandwidth by increasing the thickness of the substrate and reducing the surface waves by decreasing the thickness of the substrate. In addition, another limitation is that the bandwidth of the radiating patch using line feeding is limited to 1–5%. Therefore, to overcome all these limitations, we present a coplanar waveguide (CPW) fed semi-circular UWB antenna to enhance the impedance-bandwidth. Initially, a circular patch antenna is designed by using Eqs. (7) and (8) [26], and later modified into a semi-circular patch with a stepped stub to achieve better return loss (S_{11}) characteristics.

$$a = \frac{F}{\left(1 + \frac{2h}{\pi F \varepsilon_r}\left[\ln\left(\frac{\pi F}{2h}\right) + 1.7726\right]\right)^{1/2}} \tag{7}$$

$$F = \frac{8.791 \times 10^9}{f_r \sqrt{\varepsilon_r}} \tag{8}$$

where "a" is the radius of a circular radiator element

By employing a coplanar waveguide (CPW), feed to a semi-circular patch with a bandwidth of 7.5 GHz is achieved, and the design equations of the CPW feed are represented in Eqs. (9)–(10) [26].

$$\varepsilon_{eff} = 1 + \frac{\varepsilon_r - 1}{2}\left[\frac{K(k)}{K'(k)}\frac{K'(k_1)}{K(k_1)}\right] \tag{9}$$

$$Z_0 = \frac{30\pi}{\sqrt{\varepsilon_{eff}}}\frac{K(k)}{K'(k)} \tag{10}$$

The design and simulation analysis of the proposed UWB antenna was performed by the ANSYS HFSS tool, and a prototype model of the UWB antenna is represented in Fig. 4. An iterative design procedure of the suggested broadband UWB antenna is illustrated in Fig. 5. The suggested model was implemented in two stages. Firstly, a basic semi-circular stepped patch antenna (Antenna-1) was

(a) Front view   (b) Back view

Figure 4. Fabricated model of a semi-circular UWB antenna.
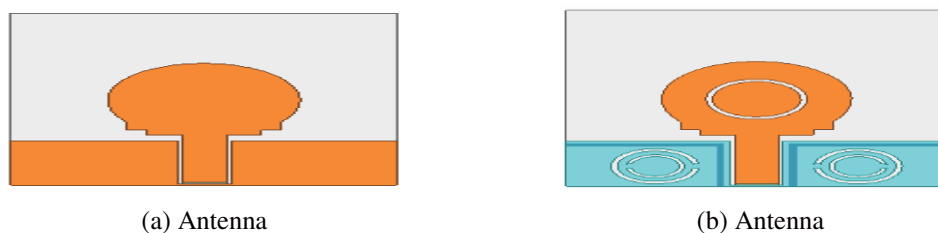

(a) Antenna   (b) Antenna

Figure 5. Iteration of a semi-circular UWB antenna.

designed with CPW feeding achieved with a $50\,\Omega$ microstrip feed line printed on the topside of the substrate shown in Fig. 5(a). Secondly, the proposed broadband UWB antenna (Antenna-2) with enhanced bandwidth designed with a circular slot was etched on the semi-circular radiator; L-shaped resonators were designed on the backside of the substrate; and a pair of complementary split ring resonators (CSRR) was etched on the two sides of the CPW feed ground plane, as shown in Fig. 5(b). This antenna covers a wide impedance bandwidth of 130.3% from 3.16 to 15 GHz with $-10\,$dB return loss.

2.3. FSS Reflector Principles Used to Increase the Gain of the Proposed Antenna

Basically, UWB antennas exhibit omnidirectional radiation, which leads to very high interference. Cavity based reflectors are used to create unidirectional radiation characteristics by redirecting the back radiation, therefore enhancing the gain of the radiators. It is clear that planar metallic reflectors cannot enhance the gain over the UWB range owing to their out of phase reflection. The advances in periodic structures have led to the development of FSS reflectors, which enhance the gain over the UWB range owing to their in-phase reflection. The side view of a UWB antenna with an FSS reflector is represented in Fig. 6(a). The compact single-layer UWBFSS reflector designed in this study consists of two square ring resonant elements shown in Fig. 6(b). By employing four branches in the two square rings, the electrical size of an entire reflector can be increased, which enhances the impedance bandwidth. The FSS model was designed on an FR4 epoxy substrate with a thickness (h_2) of 1.6 mm. The equivalent circuit model (ECM) offers a simple and fast technique for FSS analysis. The basic unit form of the designed FSS is a square loop, which can be equivalent to the LC series model [27]. Fig. 6(c) shows the equivalent circuit model of the designed FSSs. The equivalent inductance and capacitance of the circuit can be solved according to Eqs. (11)–(16) [27], where d, p, s, and g are dimensions of the square loops of t FSSs in Table 3, and θ is the incidence angle. Fig. 6(c) shows the equivalent circuit of the outer loop, where the loop contributes to the inductance, L_1, and the gap in between the two adjacent elements provides capacitance C_1. Similarly, the inductance L_2 and capacitance C_2 of the inner loop are known. According to Eqs. (11)–(16), $L_1 = 2.35\,$nH, $C_1 = 171.55\,$fF, $L_2 = 1.38\,$nH, and $C_2 = 85.775\,$fF. The resonance frequency calculated by the ECM is $f_1 = 7.92\,$GHz and $f_2 = 14.6\,$GHz, which are approximately equal to the simulated values of 7.89 GHz and 14.5 GHz represented in Fig. 7(a). At these frequencies, the reflection phase with a zero degree is achieved, which indicates that there is maximum transmission.

$$\frac{X_L}{Z_0} = \omega L = \frac{d}{p}\cos\theta F(p, 2s, \lambda) \tag{11}$$
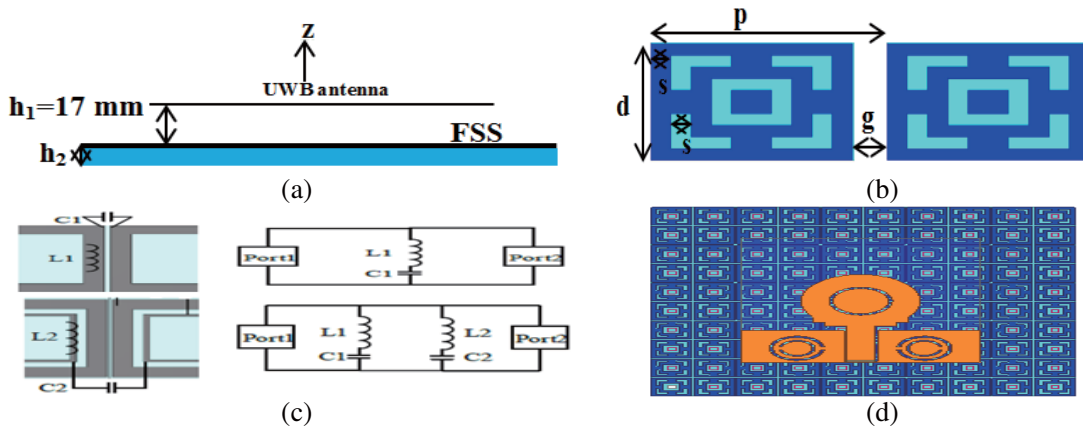

Figure 6. (a) Side view of the UWB antenna with an FSS reflector, (b) dimensions of a unit cell of the FSS element, (c) equivalent circuit model of the FSS and, (d) top view of the UWB antenna based on the FSS reflector (Antenna-3).

Table 3. Proposed UWB antenna dimensions (All the values are in mm).

Explanation of the Parameter	Value	Explanation of the Parameter	Value
Width of the substrate (W_S)	30	Width of stub1 (W_{STEP1})	12
Length of the substrate (L_S)	35	Length of stub2 (L_{STEP2})	1
Width of the ground plane (W_G)	12.9	Width of stub2 (W_{STEP2})	9
Length of the ground plane (L_G)	9	Width of the horizontal section of the "L" shaped resonator (W_1)	12.4
Length of Feed (L_F)	10.25	Length of a horizontal section of the "L" shaped resonator (L_1)	0.5
Width of Feed (W_F)	3.5	Length of a vertical section of the "L" shaped resonator (L_2)	8.5
Radius of a semi-circular patch (R_1)	7.5	Outer radius of the CSRR (r_1, r_2)	3.5, 3
Outer radius of the circular slot (R_2)	4	Inner radius of the CSRR (r_3, r_4)	2.3, 1.9
Inner radius of the circular slot (R_3)	3.5	Gap between the splits (G)	0.5
Length of stub1 (L_{STEP1})	1.5		

$$\frac{B_C}{Y_0} = \omega C = 4\frac{d}{p}\sec\theta F\left(p, g, \lambda\right)\varepsilon_{\textit{eff}} \tag{12}$$

where,

$$F\left(p, s, \lambda\right) = \frac{p}{\lambda}\left[\ln\left(\cos ec\frac{\pi s}{2p}\right) + G\left(p, s, \lambda\right)\right] \tag{13}$$

$$G\left(p, s, \lambda\right) = \frac{1}{2} \times \frac{\left(1 - \beta^2\right)^2\left[\left(1 - \frac{\beta^2}{4}\right)\left(A_+ + A_-\right) + 4\beta^2 A_+ A_-\right]}{\left(1 - \frac{\beta^2}{4}\right) + \beta^2\left(1 + \frac{\beta^2}{2} - \frac{\beta^4}{8}\right)\left(A_+ + A_-\right) + 2\beta^6 A_+ A_-} \tag{14}$$

with

$$A_{\pm} = \frac{1}{\sqrt{\left[1 \pm \frac{2p\sin\theta}{\lambda} - \left(\frac{p\cos\theta}{\lambda}\right)^2\right]}} - 1; \quad \beta = \sin\left(\frac{\pi s}{2p}\right) \tag{15}$$

$$\varepsilon_{\textit{eff}} = \frac{\varepsilon_r + 1}{2} - \frac{\varepsilon_r - 1}{2} \times \exp\left(\frac{-13h}{p}\right) - \left(\frac{100s^2}{d} - 2g + 10h\right) \tag{16}$$

The parameters of the optimized FSS unit element are listed in Table 4.

Table 4. Dimensions of the unit cell of the FSS reflector (mm).

variable	P	d	s	g
value	5.35	5	1	0.35

The reflection phase of the FSS must follow the resonance condition over the UWB range to enhance the gain of the antenna. A gap of 0.35 mm between the adjacent FSS elements is considered. The phase of the FSS unit element is shown in Fig. 7(a). A full wave analysis is performed to examine the reflection phase of a unit cell of the FSS element in Ansoft HFSS. It can be observed that the FSS possesses a dual 0° reflection phase at 7.89 GHz and 14.5 GHz. The prototype model of the proposed UWB antenna based on an FSS reflector is represented in Fig. 7(b). As the space between the FSS reflector and antenna is an integer multiple of half of the wavelength, the reflected wave is added with the exact wave that enhances the gain, which satisfies the principle of co-reflection.

The antenna is employed at a distance of 17 mm from the FSS reflector as represented in the prototype model shown in Fig. 7(b). The wave radiated by the UWB antenna is in phase with the wave
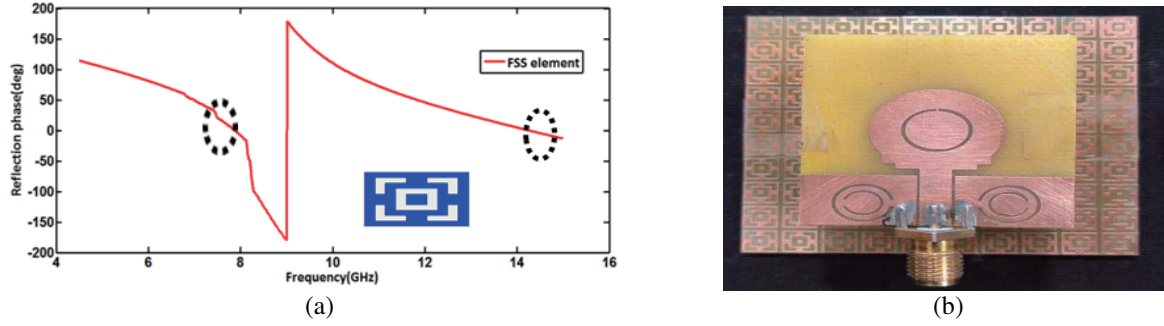
(a)   (b)

Figure 7. (a) Reflection phase and, (b) prototype model of the UWB antenna based on an FSS reflector.

reflected by the FSS reflector to improve the gain of the proposed antenna. Hence, the phase of the UWB antenna and the FSS reflector must fulfil the condition represented in Eq. (17) [28].

$$\phi_{fss} - 2\beta h_1 = 2n\pi \qquad (17)$$

where $n = -2, -1, 0, 1, 2$. Here, β is the propagation constant in the free space, ϕ_{fss} the phase of the FSS, and h_1 the separation between the FSS reflector and UWB antenna. By considering 9 GHz as the center frequency and $\phi_{fss} = 0$, h_1 is calculated as 16.64 mm, which is approximately equal to 17 mm. The FSS reflector uses 10×10 elements of size 53.15 mm×53.15 mm.

3. RESULTS AND DISCUSSION

The suggested antenna was fabricated on an FR4 Epoxy substrate with a thickness of 1.6 mm and dielectric permittivity of 4.4. Simulation of the suggested UWB antenna based on FSS reflector is done with Ansys HFSS, and the prototype is shown in Fig. 7(b).

3.1. Return Loss (S_{11}) Characteristic, VSWR and Input Impedance

The proposed antenna is described in three iterations. The basic antenna (Antenna-1) comprises a CPW-fed semi-circular stepped patch as shown in Fig. 5(a), which operates at a dual-band with an impedance bandwidth of 9.1 GHz.

Antenna-2 is modified with a circular slot, a pair of L-shaped resonators on the back end of the substrate, and CSRRs on the ground plane as shown in Fig. 5(b). The second iteration of the UWB antenna (Antenna-2) operates in broadband with an impedance bandwidth of 11.84 GHz ranging from 3.16 GHz to 15 GHz which is designed and analyzed. Finally, the proposed UWB antenna (Antenna-3) shown in Fig. 6(c) employs an FSS reflector placed at a height (h_1) of 17 mm to enhance the gain. The simulated return loss (S_{11}) characteristics of the systematic design of the suggested UWB antenna
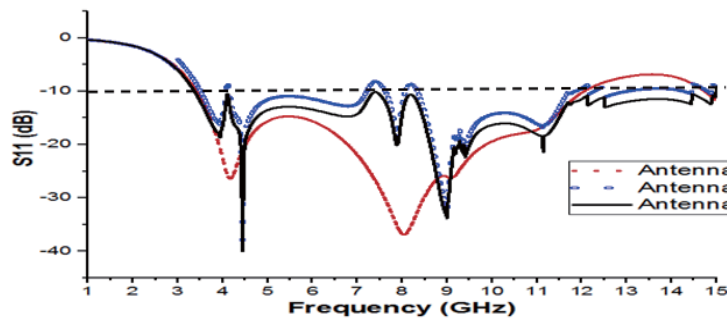

Figure 8. Return loss (S_{11}) plot of the step-by-step design of the broadband UWB antenna based on an FSS reflector.
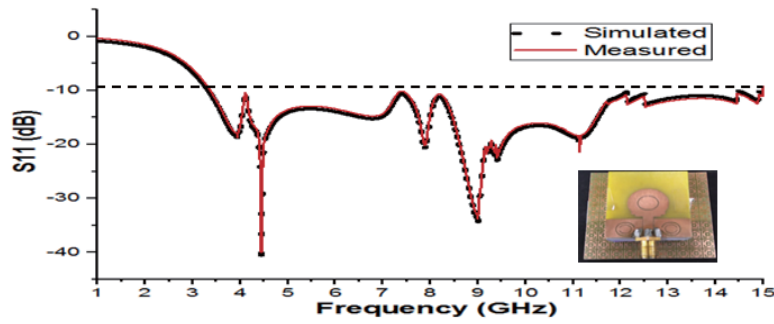
Figure 9. Simulated and measured return loss characteristics (S_{11}) of the broadband UWB antenna based on an FSS reflector.
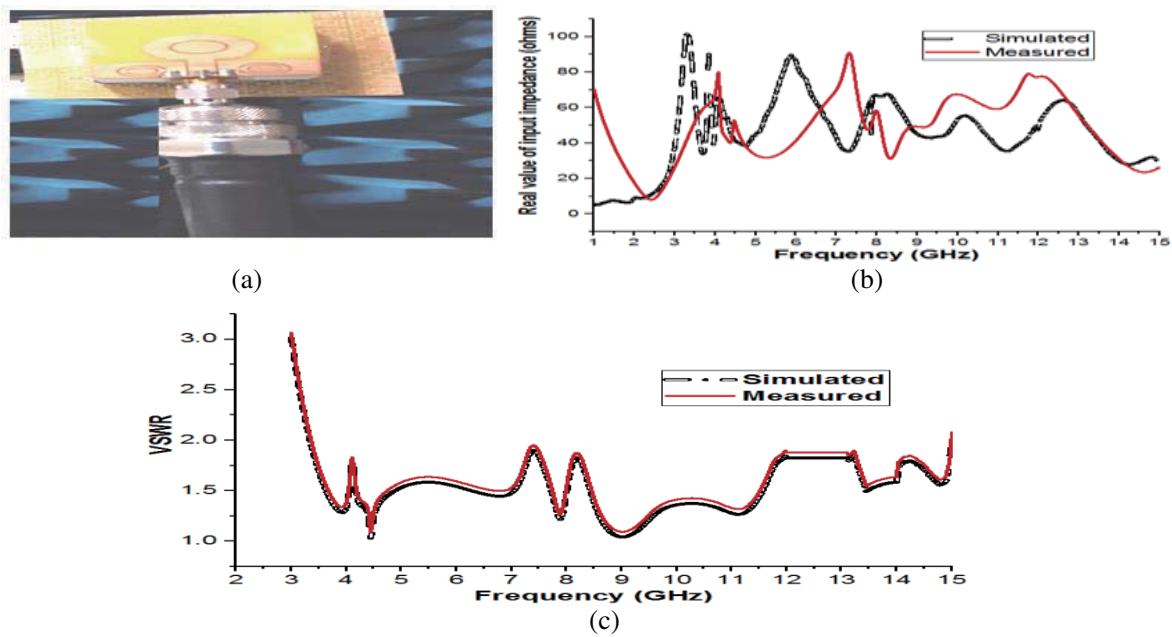

(a)

(b)

(c)

Figure 10. (a) Test set up in an anechoic chamber, (b) simulated and measured real value of input impedance and, (c) simulated and measured VSWR parameter.

based on the FSS reflector are shown in Fig. 8. A good agreement is obtained between the simulated and measured return loss characteristics (S_{11}), as shown in Fig. 9. The suggested antenna operates at 3.79 GHz, 4.44 GHz, 7.89 GHz, 9.01 GHz, and 11.15 GHz with return loss (S_{11}) of -18.2 dB, -38.7 dB, -19.4 dB, -32.5 dB, and -20.2 dB, respectively, over the entire UWB frequency range. A test set up in an anechoic chamber was obtained by using the Anritsu VNA master MS 2037C shown in Fig. 10(a). A perfect correlation can be noticed between the simulated and measured VSWRs of the recommended antenna as shown in Fig. 10(c); furthermore, it can be seen that the VSWR is less than 1.36 at all operating bands. The simulated and measured real values of the input impedance are plotted in Fig. 10(b).

3.2. Current Distributions and Radiation Patterns

The current distribution of the suggested UWB antenna based on an FSS reflector at 7.89 GHz was simulated using HFSS as shown in Fig. 11, which predicts that a strong surface current is concentrated throughout the patch and around the FSS elements placed near the radiator. It can be noticed that
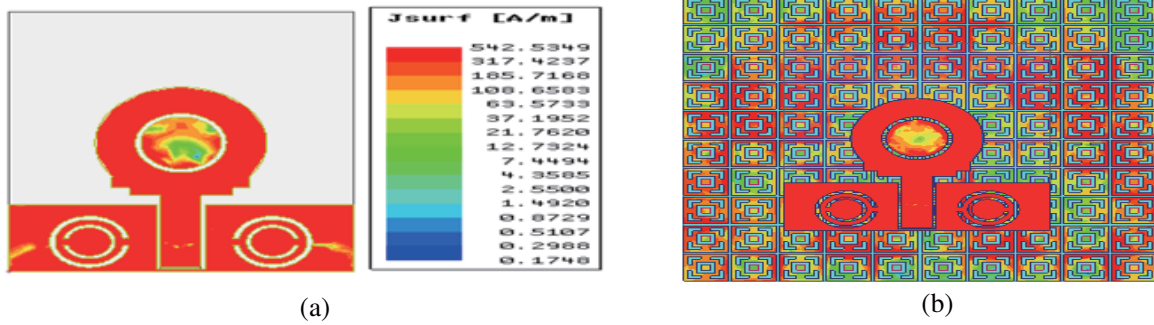
(a)   (b)

Figure 11. Surface current distributions of (a) a UWB antenna and (b) the UWB antenna based on an FSS reflector at 7.89 GHz.

at 7.89 GHz, nearly all the current is trapped around the FSS elements placed near the radiator. The FSS elements placed at the top most edges away from the radiator exhibit a lower current distribution. The E ($\phi = 0°$) and H ($\phi = 90°$) plane radiation patterns of the suggested UWB antenna based on an FSS reflector at various operating frequencies are shown in Fig. 12. In a UWB antenna, the E-plane is usually defined as the plane containing the feed line and maximum radiation of the antenna. The H-plane is the plane perpendicular to the E-plane. From the measured results, the proposed antenna has an omnidirectional radiation pattern in the H-plane at lower frequencies (3.79, 4.44, and 7.89 GHz) and is nearly omnidirectional at higher frequencies (9.01 and 11.15 GHz) with good agreement with simulations. The measured E-plane radiation patterns are similar to a dipole radiator (or) a dumbbell-shaped pattern at lower frequencies (3.79, 4.44 and 7.89 GHz). Quasi-dipole radiation patterns are noticed in the E-plane at 9.01 and 11.15 GHz. E_θ and E_ϕ are co- and cross-pol components in the E-plane whereas E_ϕ and E_θ are co- and cross-pol components in the H-plane. A perfect correlation is noticed between the simulated and measured results. The cross-pol level in the E-plane is below -40 dB while that in the H-plane it is below -15 dB. The dip occurs in the co-pol component of the E-plane at $\theta = 90°$ and $\theta = 270°$ because of finite dimensions of the ground plane.

3.3. Peak Gain and Efficiency

The peak gain of a UWB antenna with an FSS reflector (Antenna-3) is measured and compared with that of a basic UWB antenna (Antenna-2). It is observed that the average peak gain of the proposed antenna increased from 4.9 dB to 10.9 dB is achieved at all operating bands as shown in Fig. 13(a). The antenna efficiency, which is defined as the ratio of the radiated power to the power input to the antenna, is measured for the antenna using Wheeler's cap method [29] at all frequency bands.

The radiation efficiency of a UWB antenna with an FSS reflector is measured and compared with that of a basic UWB antenna without an FSS reflector; the result reveals that the efficiency is increased from 20% to 90.1% at all operating bands as shown in Fig. 13(b). In this study, a UWB antenna is designed based on an FSS reflector, which definitely enhances the antenna's efficiency, peak gain, and directivity.

3.4. Parametric Analysis by Varying Height (h_1) of FSS Reflector

The parametric analysis of a UWB antenna based on an FSS reflector is analysed as shown in Fig. 14. The FSS reflector uses 10×10 elements of size 53.15 mm×53.15 mm. When an antenna is placed at a height h_1 (mm) above the FSS, the wave radiated towards the FSS is reflected back and added to the wave radiated from the antenna. It is estimated that the gain of the antenna in the existence of the FSS reflector will be extremely high if the two wave components are added in phase. When a UWB antenna is placed at a height (h_1) of 17 mm, the gain of the antenna is drastically increased from 4.9 dB to 10.9 dB over the entire UWB range in the presence of the FSS reflector.
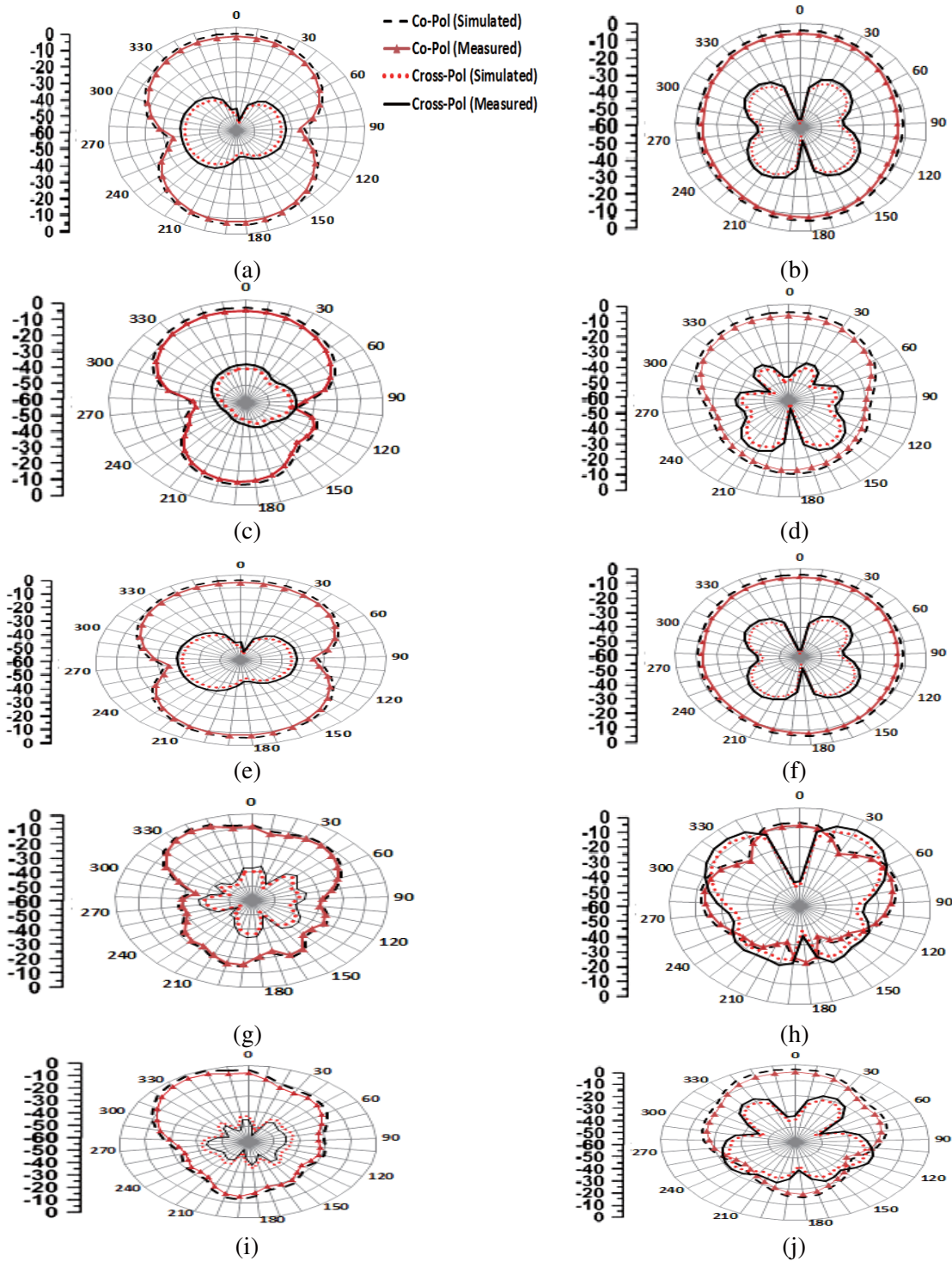
Figure 12. Measured and simulated radiation patterns of the suggested FSS reflector based UWB antenna: (a) E-plane (XZ plane) at a frequency of 3.94 GHz, (b) H-plane (YZ plane) at a frequency of 3.94 GHz, (c) E-plane (XZ plane) at a frequency of 4.44 GHz, (d) H-plane (YZ plane) at a frequency of 4.44 GHz, (e) E-plane (XZ plane) at a frequency of 7.89 GHz , (f) H-plane (YZ plane) at a frequency of 7.89 GHz, (g) E-plane (XZ plane) at a frequency of 9.01 GHz, (h) H-plane (YZ plane) at a frequency of 9.01 GHz, (i) E-plane (XZ plane) at a frequency of 11.15 GHz, and (j) H-plane (YZ plane) at a frequency of 11.15 GHz.
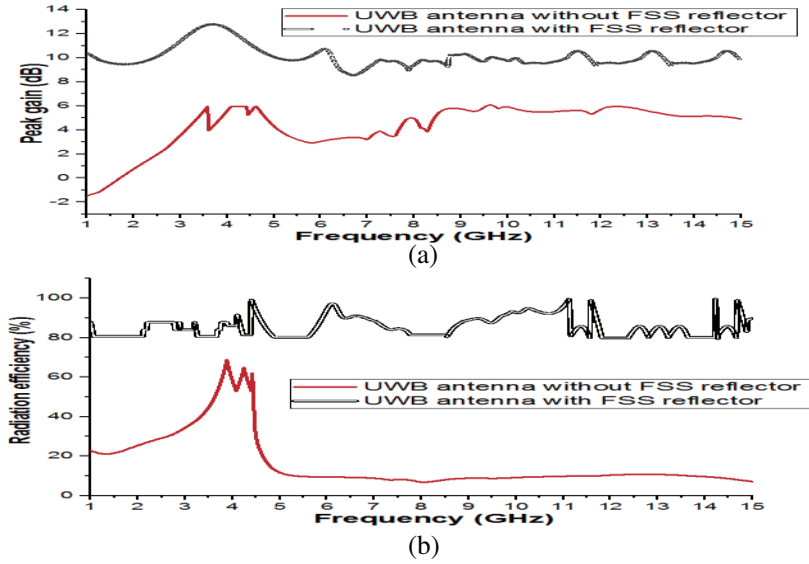
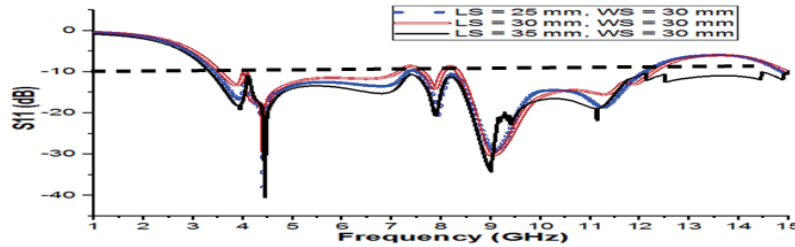**Figure 13.** Frequency plots of the (a) peak gain and (b) radiation efficiency for the suggested antenna.

Figure 14. Peak gain of the proposed antenna by varying the height (h_1) of the FSS reflector.

3.5. Parametric Analysis of the UWB Antenna with Various Dimensions (L_S and W_S) of the Ground Plane

Parametric analysis of the UWB antenna of FR4 epoxy of thickness $h = 1.6$ mm based on the dimensions (L_S and W_S) of ground planes with different L_S values of 25 mm, 30 mm, and 35 mm are performed, and the results are shown in Fig. 15. This indicates that if we choose the dimensions of the ground plane as $L_S = 35$ mm and $W_S = 30$ mm, then an impedance bandwidth of 130.3% from 3.16 to 15 GHz with a -10 dB return loss is achieved.
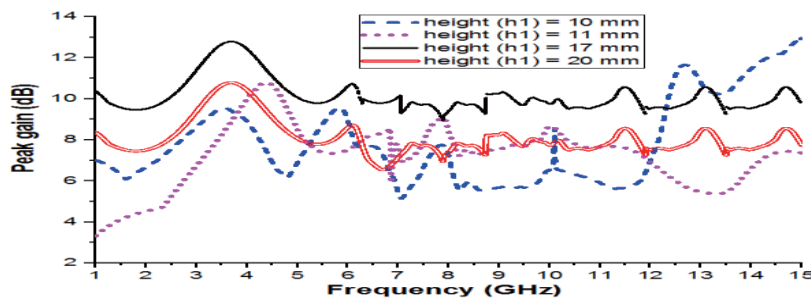

Figure 15. Return loss (S_{11}) plot for the UWB antenna based on the dimensions of the ground plane.

4. TIME RESPONSE ANALYSIS OF THE PROPOSED UWB ANTENNA BASED ON A FSS REFLECTOR

A high degree of correlation between the transferred signal and received signal in wireless communication plays a prominent role in reducing losses in the modulated signal. To determine the pulse performance characteristics of the suggested FSS reflector-based UWB antenna, two identical antennas are employed in side-to-side and face-to-face scenarios but placed 50 cm apart, which is three times of the wavelength of the lowest operating frequency (3.79 GHz). This satisfies the far-field radiation conditions shown in Fig. 16(a) and Fig. 17(a).
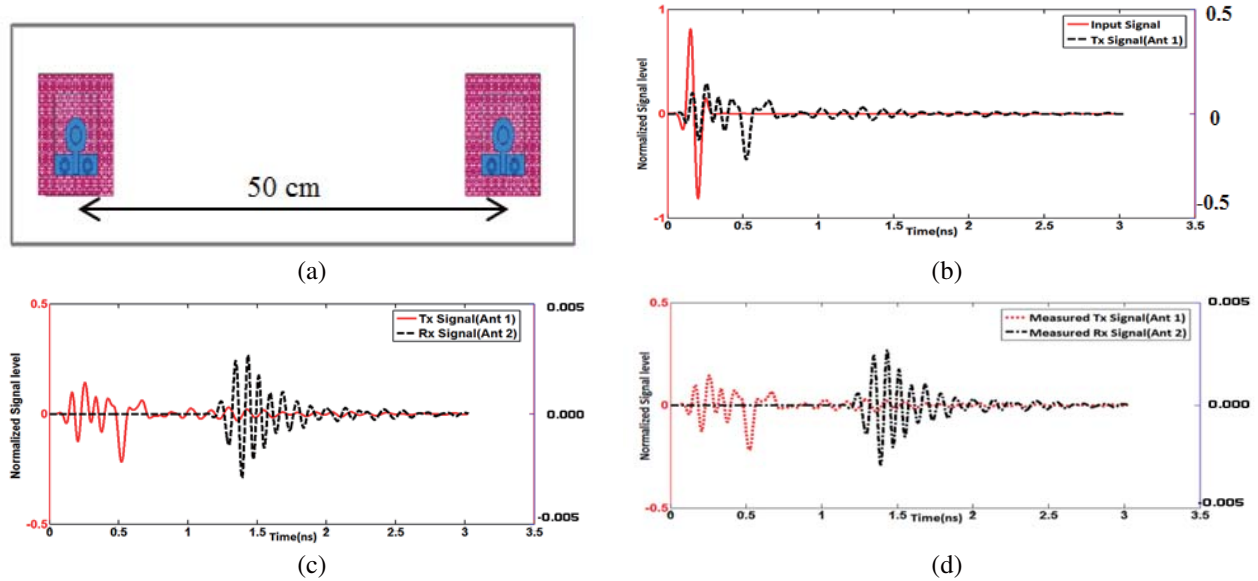

Figure 16. Time domain analysis: (a) Side-by-side scenario placed apart by 50 cm and the normalized signal levels of the (b) input and transmitted signals, (c) transmitted and received signals, and (d) measured transmitted and received signals.

4.1. Side-to-Side Scenario

The signal source uses a modulated Gaussian pulse, and the corresponding spectrum is 3.16–15 GHz. The normalized amplitudes of the transmitted and received pulses are presented. It can be seen from Fig. 16(d) and Fig. 17(d) that the received signal is very similar to the transmitted pulse.

At the same time, the distortion of the pulse is quantitatively evaluated using the fidelity factor, F [30]. The correlation [30] (fidelity factor) between the two signals is calculated from Eqn. (18) as:

$$F = Max_\tau \left| \frac{\int_{-\infty}^{+\infty} Z(t) r(t-\tau) dt}{\sqrt{\int_{-\infty}^{+\infty} Z(t)^2 dt \int_{-\infty}^{+\infty} r(t)^2 dt}} \right| \tag{18}$$

Here, $Z(t)$ is the modulated signal, and $r(t)$ is the received signal. For the side-to-side scenario, the fidelity factors achieved for the input and transmitted signals, and the transmitted and received signals are 90% and 86%, respectively, whereas the measured result is 84%.

4.2. Face-to-Face Scenario

For the face-to-face scenario, the fidelity factor achieved for the transmitted to received signal is 78% of the correlation, whereas the measured result is 76%. The higher the cross-correlation is between the transmitted and received signals, the better the signal fidelity is.
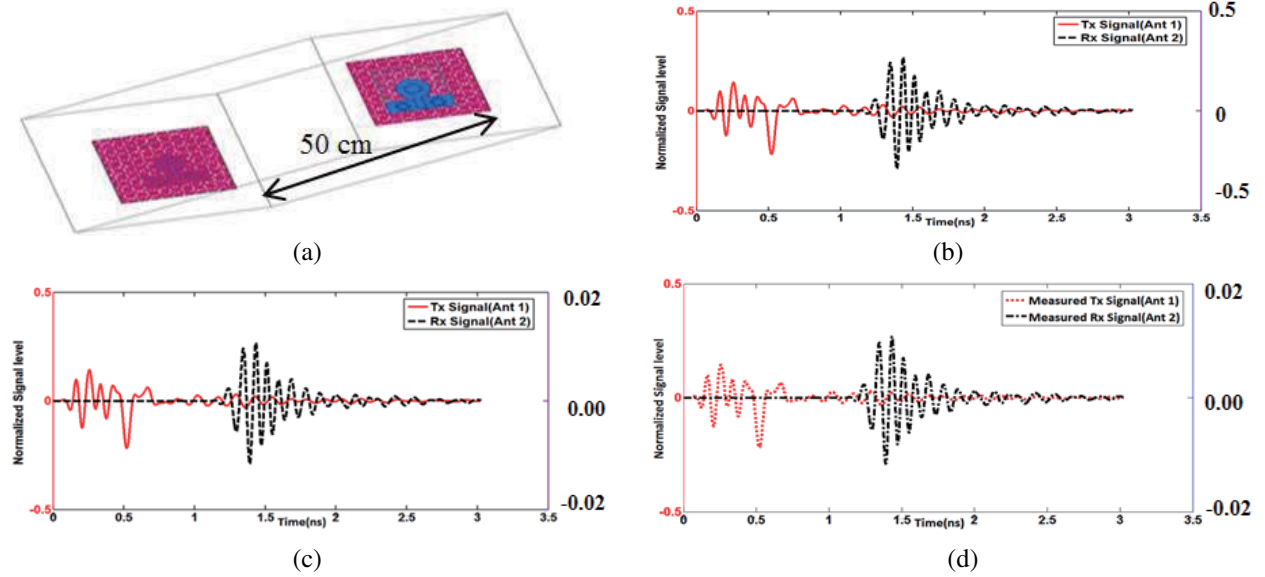
Figure 17. Time domain analysis: (a) Face-to-face scenario placed apart by 50 cm and the normalized signal levels of the (b) input and transmitted signals, (c) transmitted and received signals, and (d) measured transmitted and received signals.

The performance characteristics of the proposed antenna, i.e., the resonant frequency (GHz), return loss (S_{11}) in decibel, VSWR, input impedance (Ω), and peak gain (dB), are listed in Table 5.

Table 5. Performance characteristics of the proposed work.

Proposed work	Resonant Frequencies (GHz)	Return loss Characteristics, S_{11} (dB)	VSWR	Input Impedances (Ω)	Peak Gain (dB)	Radiation Efficiency (%)
UWB	3.79	−18.2	1.36	41.7	13.54	90
antenna	4.44	−38.7	1.15	48.86	10.25	96.64
based on	7.89	−19.4	1.35	42.20	10.98	89.79
FSS	9.01	−32.5	1.19	45.49	11.27	91.98
reflector	11.15	−20.2	1.31	43.08	10.9	90.13

5. CONCLUSION

A novel UWB antenna based on an FSS reflector with an enhanced impedance-bandwidth designed using a CSRR and an L-shaped resonator operates at 3.79 GHz, 4.44 GHz, 7.89 GHz, 9.01 GHz, and 11.15 GHz frequency bands with return losses (S_{11}) of −18.2 dB, −38.7 dB, −19.4 dB, −32.5 dB, and −20.2 dB respectively. The dimensions of the CPW-fed UWB antenna are 35×30×1.6 mm^3, and those of the UWB antenna with an FSS reflector, which consists of 10×10 array of elements located at a distance of 17 mm below the proposed antenna, are 53.15×53.15×1.6 mm^3. Firstly, a UWB antenna employing a pair of L-shaped resonators and CSRRs is proposed which provides a wide impedance bandwidth of 130.3% from 3.16 to 15 GHz with −10 dB return loss. Finally, an FSS reflector is employed below the suggested UWB antenna to enhance the gain from 4.9 dB to 10.9 dB. The suggested antenna presents an omnidirectional radiation pattern in the H-plane at lower frequency bands, a quasi-omnidirectional radiation pattern at upper bands, and a dumbbell pattern similar to a dipole antenna in the E-plane

for the complete UWB range. Time response analysis was performed for the proposed antenna. The prototype model of the antenna was fabricated, and the experimental results demonstrated perfect agreement with the simulated ones.

REFERENCES

1. Mobashsher, A. T. and A. Abbosh, "Utilizing symmetry of planar ultra-wideband antennas for size reduction and enhanced performance," *IEEE Antennas Propag. Mag.*, 2015.

2. Liu, Y., et al., "Some recent developments of microstrip antenna," *International Journal of Antennas and Propagation*, 2012.

3. Cicchetti, R., A. Faraone, D. Caratelli, and M. Simeoni, "Wideband, multiband, tunable, and smart antenna systems for mobile and UWB wireless applications," *International Journal of Antennas and Propagation*, 2013.

4. First report and order. Revision of part 15 of the commission's rule regarding, "Ultra wide band transmission system FCC 02-48," Federal Communications Commission, 2002.

5. Aiello, G. R. and G. D. Rogerson, "Ultra-wideband wireless systems," *IEEE Microw. Mag.*, 2003.

6. Liu, W. X., Y. Z. Yin, W. L. Xu, and S. L. Zuo, "Compact open-slot antenna with bandwidth enhancement," *IEEE Antennas Wirel. Propag. Lett.*, 2011.

7. Sung, Y., "Bandwidth enhancement of a microstrip line-fed printed wide-slot antenna with a parasitic center patch," *IEEE Trans. Antennas Propag.*, 2012.

8. Xu, K., Z. Zhu, H. Li, J. Huangfu, C. Li, and L. Ran, "A printed single-layer UWB monopole antenna with extended ground plane stubs," *IEEE Antennas Wirel. Propag. Lett.*, 2013.

9. Dastranj, A. and F. Bahmanzadeh, "A compact UWB antenna design using rounded inverted L-shaped slots and beveled asymmetrical patch," *Progress In Electromagnetics Research C*, Vol. 80, 131–140, 2018.

10. Siddiqui, J. Y., C. Saha, and Y. M. M. Antar, "A novel ultrawideband (UWB) printed antenna with a dual complementary characteristic," *IEEE Antennas Wirel. Propag. Lett.*, 2015.

11. Sahoo, S., M. N. Mohanty, and L. P. Mishra, "Bandwidth improvement of compact planar antenna for UWB application with dual notch band performance using parasitic resonant structure," *Progress In Electromagnetics Research*, Vol. 66 29–39, 2018.

12. Ram Krishna, R. V. S. and R. Kumar, "Slotted ground microstrip antenna with FSS reflector for high-gain horizontal polarisation," *Electron. Lett.*, 2015.

13. Yahya, R., A. Nakamura, M. Itami, and T. A. Denidni, "A novel UWB FSS-based polarization diversity antenna," *IEEE Antennas Wirel. Propag. Lett.*, 2017.

14. Kundu, S., A. Chatterjee, S. K. Jana, and S. K. Parui, "A compact umbrella-shaped UWB antenna with gain augmentation using frequency selective surface," *Radioengineering*, 2018.

15. Ranga, Y., K. P. Esselle, L. Matekovits, and S. G. Hay, "Increasing the gain of a semicircular slot UWB antenna using an FSS reflector," *Proceedings of the 2012 IEEE-APS Topical Conference on Antennas and Propagation in Wireless Communications, APWC'12*, 2012.

16. Majidzadeh, M., C. Ghobadi, and J. Nourinia, "Novel single layer reconfigurable frequency selective surface with UWB and multi-band modes of operation," *AEU — Int. J. Electron. Commun.*, 2016.

17. Ranga, Y., L. Matekovits, K. P. Esselle, and A. R. Weily, "Multioctave frequency selective surface reflector for ultrawideband antennas," *IEEE Antennas Wirel. Propag. Lett.*, 2011.

18. Hussain, T., Q. Cao, J. K. Kayani, and I. Majid, "Miniaturization of frequency selective surfaces using 2.5-D Knitted structures: Design and synthesis," *IEEE Trans. Antennas Propag.*, 2017.

19. Saleem, R., M. Bilal, T. Shabbir, and M. F. Shafique, "An FSS-employed UWB antenna system for high-gain portable devices," *Microw. Opt. Technol. Lett.*, 2019.

20. Mondal, K., D. Chanda Sarkar, and P. P. Sarkar, "5×5 matrix patch type frequency selective surface based miniaturized enhanced gain broadband microstrip antenna for WLAN/WiMAX/ISM band applications," *Progress In Electromagnetics Research C*, Vol. 89 207–219, 2019.

21. Kundu, S., A. Chatterjee, S. K. Jana, and S. K. Parui, "A high gain dual notch compact UWB antenna with minimal dispersion for ground penetrating radar application," *Radioengineering*, 2018.

22. Baena, J. D., et al., "Equivalent-circuit models for split-ring resonators and complementary split-ring resonators coupled to planar transmission lines," *IEEE Trans. Microw. Theory Tech.*, Vol. 53, No. 4II, 1451–1460, 2005.

23. Ouedraogo, R. O., S. M. Ellison, J. L. Frasch, P. Chahal, and E. J. Rothwell, "Analysis of the Nicolson-Ross-Weir method for characterizing the electromagnetic properties of engineered materials," *Progress In Electromagnetics Research*, Vol. 157 31–47, 2016.

24. Numan, A. B. and M. S. Sharawi, "Extraction of material parameters for metamaterials using a full-wave simulator [education column]," *IEEE Antennas Propag. Mag.*, 2013.

25. Samson Daniel, R., R. Pandeeswari, and S. Raghavan, "Offset-fed complementary split ring resonators loaded monopole antenna for multiband operations," *AEU — Int. J. Electron. Commun.*, 2017.

26. Garg, R., P. Bhartia, I. Bahl, and A. Ittipiboon, *Microstrip Antenna Design Handbook*, 2001.

27. Langley, R. J. and E. A. Parker, "Equivalent circuit model for arrays of square loops," *Electron. Lett.*, 1982.

28. Kushwaha, N. and R. Kumar, "High gain UWB antenna using compact multilayer FSS," *IEEE MTT-S International Microwave and RF Conference 2014, IMaRC 2014 — Collocated with International Symposium on Microwaves, ISM 2014*, 2015.

29. Pozar, D. M. and B. Kaufman, "Comparison of three methods for the measurement of printed antenna efficiency," *IEEE Trans. Antennas Propag.*, 1988.

30. Quintero, G., J. F. Zurcher, and A. K. Skrivervik, "System fidelity factor: A new method for comparing UWB antennas," *IEEE Trans. Antennas Propag.*, 2011.